Supplementary Materials

Interfacial Electron Spillover Modulated Cu^{+}–$Ti^{4-\delta}$ Active Sites Facilitating Nitrate Hydrogenation for Photoelectrochemical Ammonia Synthesis

*Jingfu Sun#, Zhen Liu#, Xi Han, Huibin Li, Huige Zhang, Zhiheng Wang, Jinlong Zhang, Yipeng Guo, Jianbo Li and Yaoguang Yu**

School of Materials,

Shenzhen Campus of Sun Yat-sen University,

No. 66, Gongchang Road, Shenzhen, Guangdong 518107, P. R. China

Email: yuyg5@mail.sysu.edu.cn

Chemicals and reagents

Tetrabutyl titanate ($Ti(OC_4H_9)_4$), hydrochloric acid (HCl), sodium fluoride (NaF), sodium hydroxide (NaOH), copper sulfate ($CuSO_4$), ethanol(C_2H_5OH), potassium nitrate (KNO_3), potassium hydroxide (KOH), sodium salicylate ($C_7H_5NaO_3$), sodium nitroferricyanide ($Na_2[Fe(CN)_5NO]$), sodium hypochlorite (NaClO), sodium citrate ($Na_3C_6H_5O_7$) p-aminobenzenesulfonamide($C_6H_8N_2O_2S$), phosphoric acid (H_3PO_4), N-(1-Naphthyl) ethylenediamine dihydrochloride($C_{12}H_{14}N_2 \cdot 2HCl$) and potassium nitrite (KNO_3) were purchased were purchased from Macklin Biochemical Co. Ltd. All reagents and solvents were analytical grade. Deionized (DI) water was used during the experiments.

Materials preparation

Preparation of TiO_2. The typical synthesis process is as follows: 1 mL of tetrabutyl titanate was dissolved in a mixture of 12.5 mL hydrochloric acid (HCl) and 17.5 mL deionized water. After stirring for 10 minutes, 0.25 g of sodium fluoride (NaF) was added. The resulting solution was then transferred into a 50 mL polytetrafluoroethylene (PTFE) liner containing a fluorine-doped tin oxide (FTO) substrate (2×2.5 cm^2) with its conductive side facing downward. The liner was placed in a hydrothermal autoclave and maintained at 150 °C for 6 hours. After hydrothermal treatment, the FTO substrate was taken out, cleaned sequentially with deionized water and anhydrous ethanol, and dried at 80 °C. Subsequently, calcination was performed in a muffle furnace at 450 °C for 2 hours with a heating rate of 5 °C/min to obtain the titanium dioxide (TiO_2) substrate.

Preparation of Cu/TiO_2 Photoelectrodes. 0.1197 g of copper sulfate ($CuSO_4$) was dispersed in 50 mL deionized water to form an electrolyte. A TiO_2 substrate with a size

of 1.25×2 cm^2 was clamped as the working electrode for electrodeposition at a constant potential of -0.5 V vs Ag/AgCl. By controlling different electrodeposition durations, Cu/TiO_2-L, Cu/TiO_2-M and Cu/TiO_2-H catalyst series were prepared. The as-prepared samples were washed with ethanol and distilled water, followed by drying at 60 °C to obtain the target catalysts.

Photoelectrochemical Nitrate Reduction Reaction

PEC NO_3RR performance tests were conducted using a three-electrode system on a CHI 660E electrochemical workstation in an H-type electrolytic cell. The working electrodes were TiO_2, Cu/TiO_2-L, Cu/TiO_2-M and Cu/TiO_2-H, respectively. A platinum (Pt) electrode was used as the counter electrode, and a silver/silver chloride (Ag/AgCl) electrode served as the reference electrode. The electrolyte in the cathode chamber consisted of 0.1 mol/L potassium nitrate (KNO_3) and 0.1 mol/L potassium hydroxide (KOH). All electrolytes were purged with argon (Ar) for 30 minutes prior to PEC tests to remove dissolved oxygen. A 300 W xenon lamp was used as the light source to irradiate the photocathode. If not specified, all linear voltammetry scanning curves (LSV) are corrected for iRs compensation, where Rs is the solution resistance (Ω) between the working electrode and the reference electrode.

Characterization

Powder X-ray diffraction (XRD) patterns were r performed with a Bruker D8 advanced diffractometer with Cu Kα X-ray source (λ = 1.5406 Å). The transmission electron microscopy (TEM) and high-resolution TEM (HRTEM) images were taken on a JEM-F200 transmission electron microscope operated at 200 kV. Scanning transmission microscopy (SEM) measurements were conducted on Helios 5 CX. X-ray

photoelectron spectroscopy (XPS) tests were performed on Kratos Supra+ with Al-Kα radiation system. The calibration of XPS spectra was performed by using the C 1s peak at 284.8 eV. X-ray absorption spectroscopy (XAS) tests were conducted in a fluorescence mode at beamline X-ray absorption fine structure (XAFS) of Shanghai Synchrotron Radiation Facility (SSRF). In-situ attenuated total reflectance-Fourier transform infrared (ATR-FTIR) spectra were acquired on a Bruker VERTEX 70 based on the absorption mode equipped. The photoelectrochemical performances were measured with a CHI660E electrochemical workstation (Shanghai Chenhua Instruments).

Product detection of NO_3RR

Determination of ammonia. The concentration of NH_3 was spectrophotometrically determined by using the indophenol blue method. Typically, 2 mL of pre-diluted electrolyte were taken out and mixed with 2 mL of 1 M NaOH solution containing 5 wt.% of salicylic acid and 5 wt.% of sodium citrate. Then, the above solution was mixed with 1 mL of 0.05 M NaClO solution and 0.2 mL of an aqueous solution of 1 wt.% sodium nitroprusside. After the above mixture was kept in the dark for 2 h, the absorption spectrum was acquired using an UV-vis spectrophotometer (Hitachi UH530) at the wavelength of 654 nm. The calibration curve of ammonia concentration and absorbance was prepared by using a series of standard NH_4Cl solutions.

Determination of nitrite. Firstly, 4 g of p-aminobenzenesulfonamide, 0.2 g of N-(1-Naphthyl) ethylenediamine dihydrochloride, and 10 mL of phosphoric acid (ρ = 1.70 g/mL) were added into 50 mL of ultrapure water. After ultrasonication for about 2 mins,

the obtained transparent solution was used as the color reagent. Then, 5 mL of dilution electrolyte were mixed with 0.1 mL of color regent. After 20 mins, the absorption spectrum was taken by using an UV-vis spectrophotometer (Hitachi UH530) at the wavelength of 540 nm. A series of standard potassium nitrite solutions were prepared to obtain the calibration curve.

Calculation of the Faradaic efficiency (FE) and yield rate (R)

In this work, the FE of NH_3 or NO_2^- was calculated as follows:

$$FE_{NH_3} = (8 \times F \times C_{NH_3} \times V)/(M_{NH_3} \times Q) \times 100\%$$

$$FE_{NO^-_2} = (2 \times F \times C_{NO_2^-} \times V)/(M_{NO_2^-} \times Q) \times 100\%$$

The yield rate of NH_3 was calculated according to the following equation:

$$R_{NH_3} = (C_{NH_3} \times V)/(m_{cat} \times t)$$

where F is the Faraday constant (96485 C mol^{-1}), C_{NO2-} and C_{NH3} represent the concentration of NO_2^- and NH_3 (mg/L), V is the volume of the electrolyte (L), M_{NO2-} and M_{NH3} denote the molar mass of NO_2^- and NH_3 (mg/mol), Q is the total amount of charge (C), m_{cat} is the total amount of catalyst (mg), and t is the potentiostatic test time (h).

Photoelectrochemical in situ FTIR tests

The in-situ attenuated-total-reflectance FTIR spectroscopy with a range of 400–4000 cm^{-1} was acquired by using a Bruker VERTEX 70 spectrometer. In the measurement cell, the Cu/TiO_2 photoelectrode was the working electrode, and a platinum wire and an Ag/AgCl electrode were used as the counter and reference electrodes, respectively. The electrolyte in the cathode chamber consisted of 0.1 mol/L

potassium nitrate (KNO_3) and 0.1 mol/L potassium hydroxide (KOH). The background spectrum was taken under dark and open-circuit conditions. The in-situ FTIR spectra were collected for the photoelectrode during PEC NO_3RR under light irradiation (Xenon arc lamp) with applied bias ranging from –0.20 V to –0.80 V vs RHE.

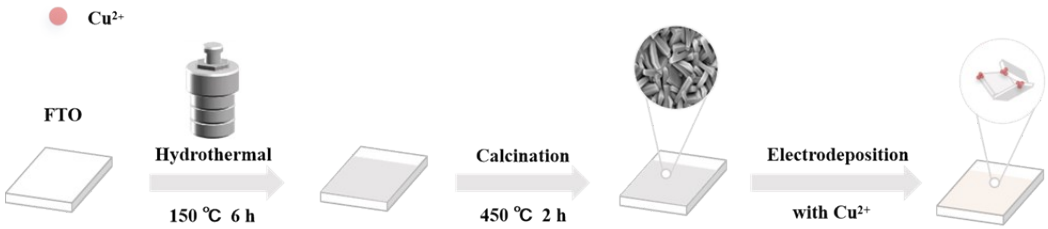

Figure S1. Synthetic route of Cu/TiO_2 photoelectrodes.

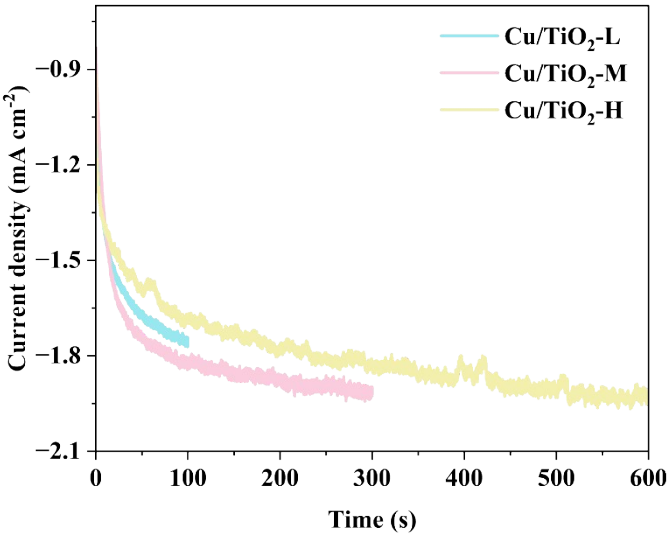

Figure S2. The *i-t* curve of the Cu/TiO_2 photoelectrodes.

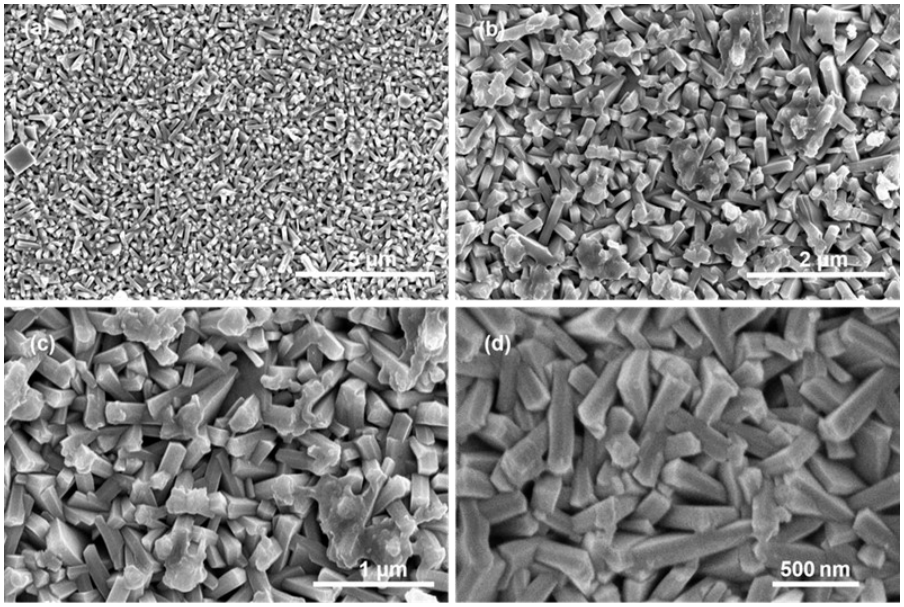

Figure S3. SEM image of Cu/TiO_2-M photoelectrode.

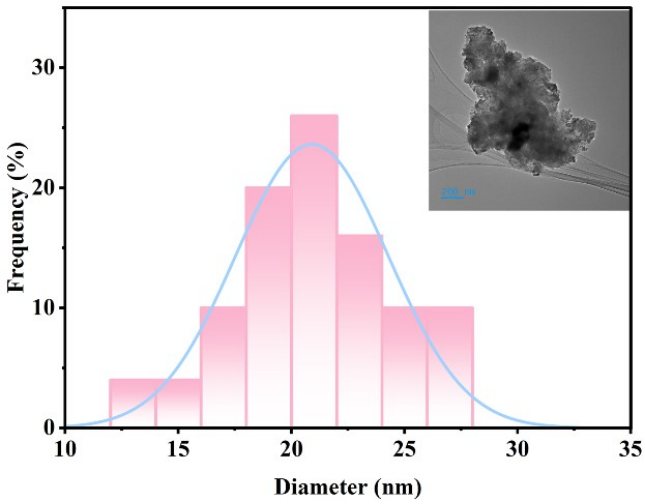

Figure S4. Particle size distribution of Cu/TiO_2-M photoelectrode.

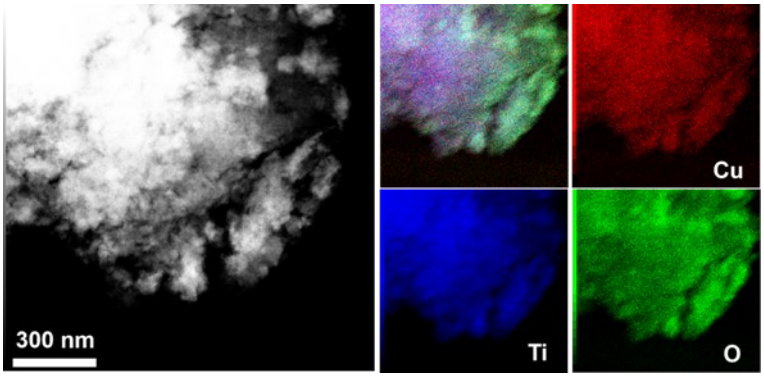

Figure S5. TEM image and the corresponding EDS elemental mappings of Cu/TiO_2-M photoelectrode.

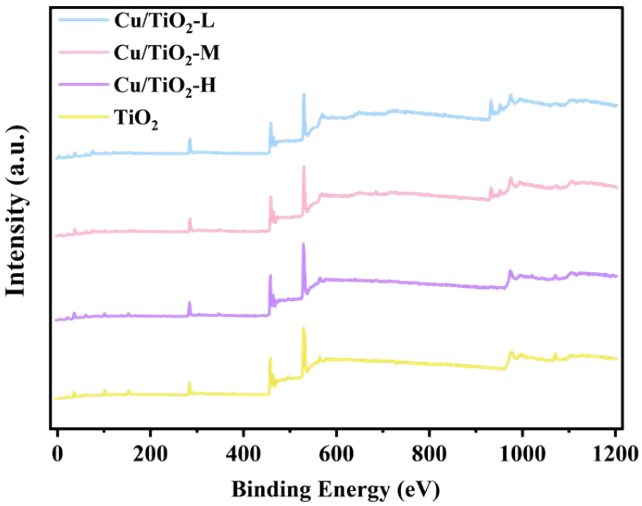

Figure S6. XPS survey spectrum of Cu/TiO_2 photoelectrodes.

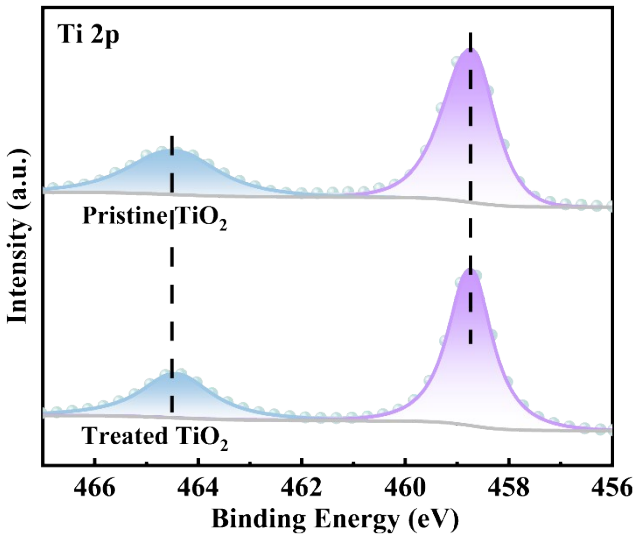

Figure S7. Ti 2p XPS spectra of TiO_2 with and without electrodeposition process.

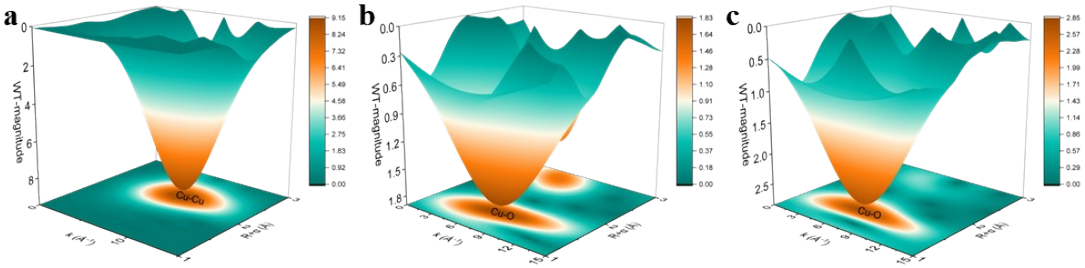

Figure S8. WT for k^3-weighted Cu K-edge EXAFS signals of (a) Cu foil and (b) Cu_2O and (c) Cu/TiO_2-M photoelectrode.

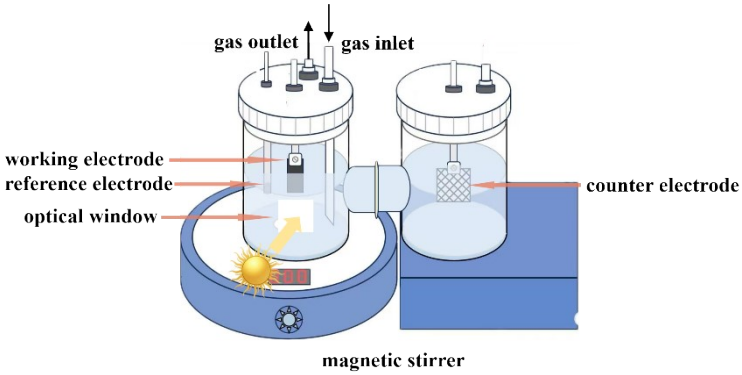

Figure S9. Schematic illustration of a standard three-electrode photoelectrochemical cell.

Figure S10. The UV-vis standard curve of NH_3 with different concentrations of NH_4Cl solutions as standards. (a) UV-vis curves of assays with NH_4^+ ions and (b) linear fitting results of the calibration curve.

Figure S11. The UV-vis standard curve of NO_2^- with different concentrations of KNO_2 solutions as standards. (a) UV-vis curves of assays with NO_2^- ions and (b) linear fitting results of the calibration curve.

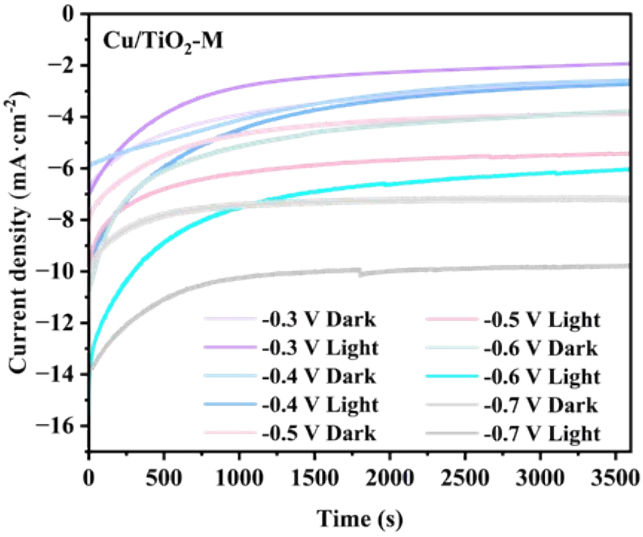

Figure S12. Comparison of i-t Curves under Light and Dark Conditions at Different Bias Voltages of Cu/TiO_2-M photoelectrode.

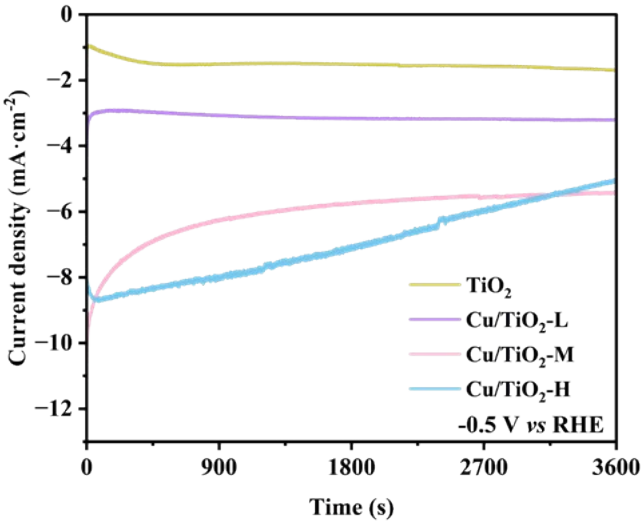

Figure S13. Comparison of i-t Curves of Cu/TiO_2 photoelectrodes at -0.5 V (vs RHE).

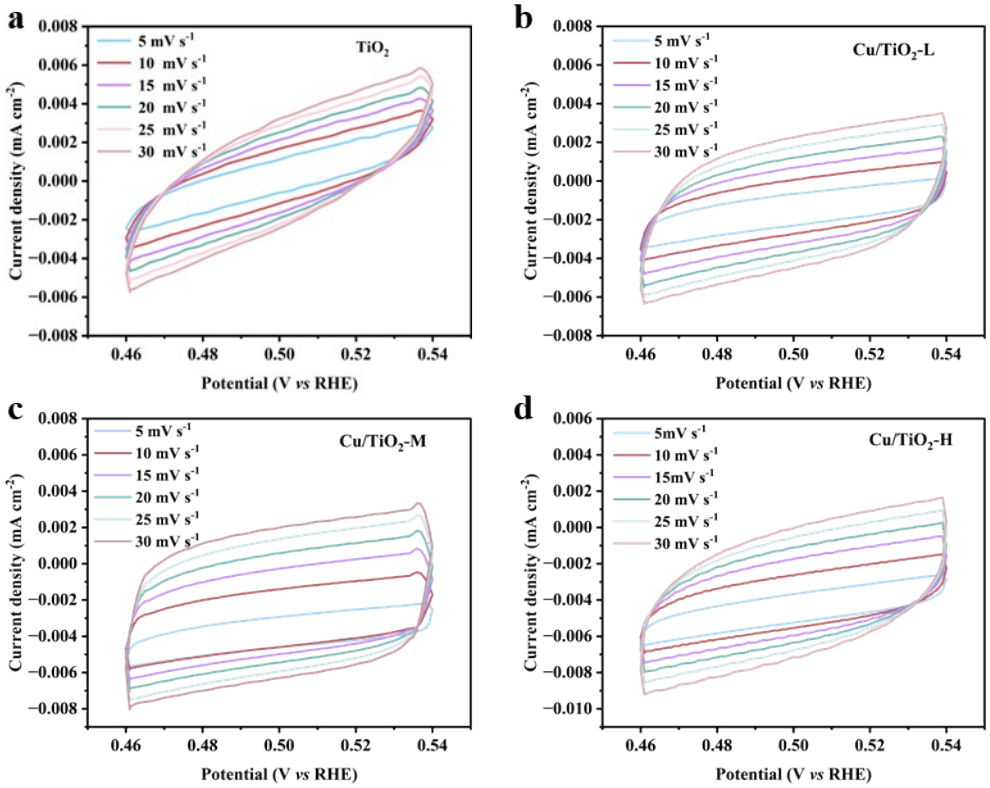

Figure S14. CV Curves at Different Scan Rates of Cu/TiO_2 photoelectrodes.

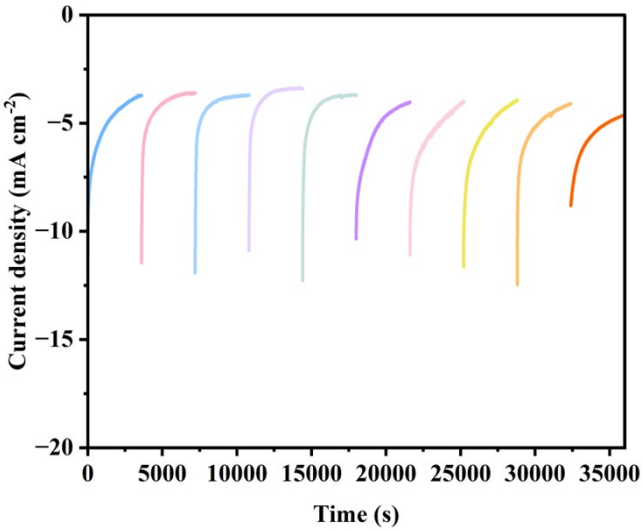

Figure S15. The chronoamperometry curves of Cu/TiO_2-M photoelectrode during the 10 consecutive electrolysis cycles at -0.5 V (vs RHE).

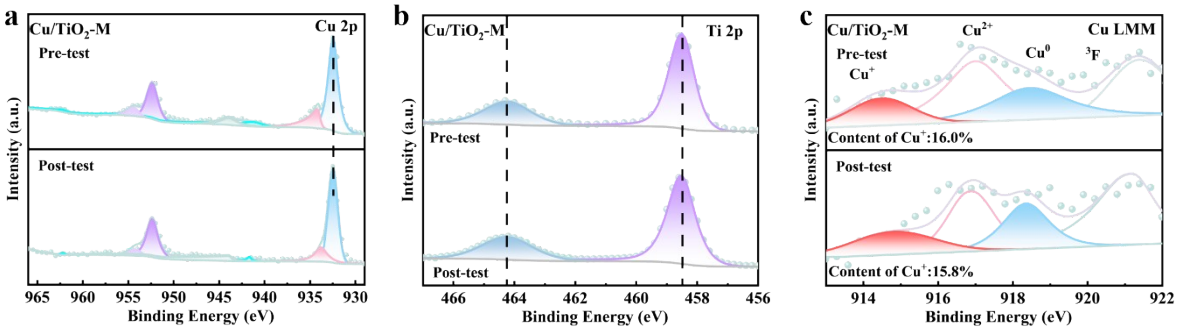

Figure S16. (a) high-resolution Cu 2p XPS spectra, (b) Cu LMM Auger electron spectra, (c) high-resolution Ti 2p XPS spectra before and after the catalytic process.

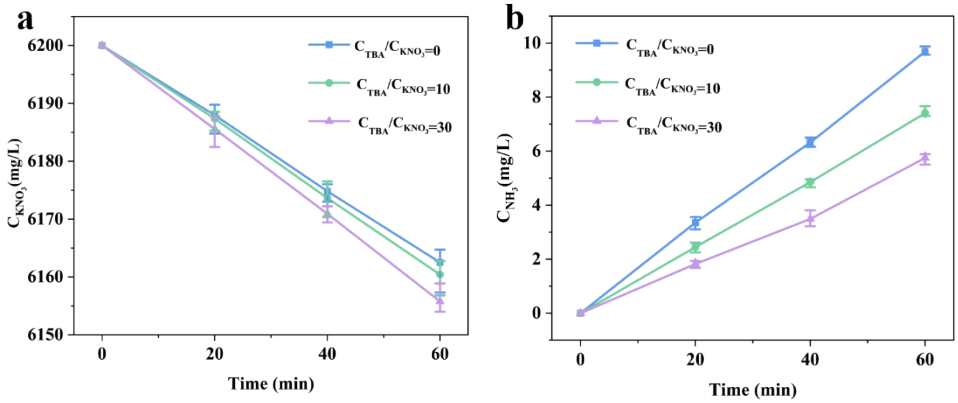

Figure S17. Effect of different ratios of C_{TBA}/C_{KNO3} on (a) NH_3 Formation and (b) KNO_3 Consumption over Cu/TiO_2-M at −0.5 V vs. RHE.

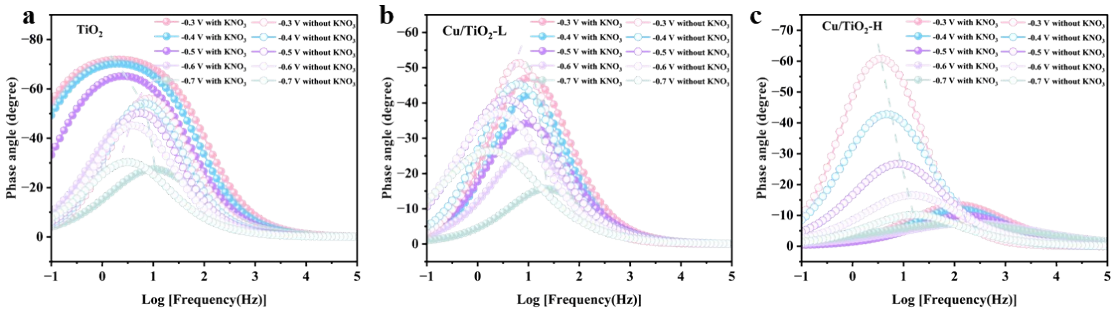

Figure S18. Bode phase plots of TiO_2, Cu/TiO_2-L and Cu/TiO_2-H at varied potentials in 0.1 M KOH and 0.1 M KNO_3 solution

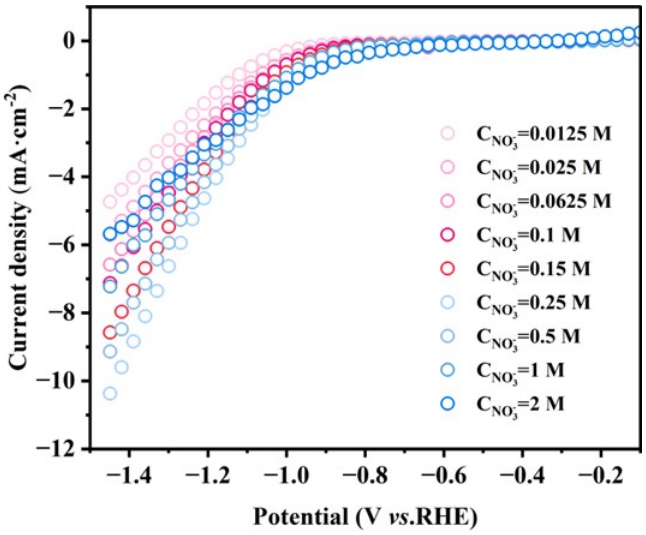

Figure S19. Comparison of LSV curves in KNO_3/KOH electrolytes with varying ratios of Cu/TiO_2-M photoelectrode.

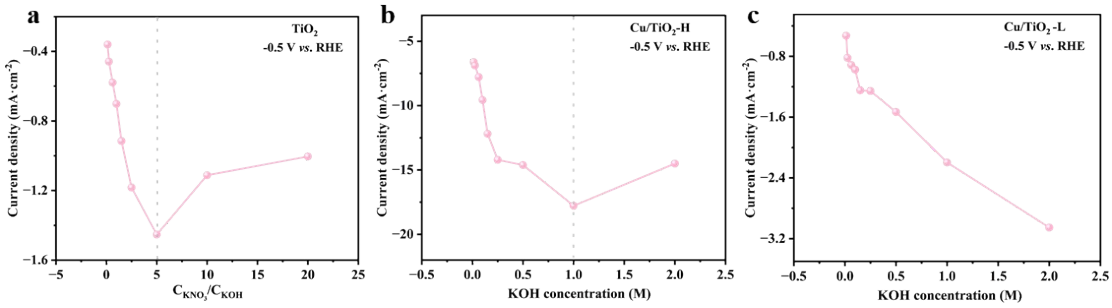

Figure S20. The effect of C_{KNO3}/C_{KOH} on current density at −0.5 V vs. RHE over TiO_2, Cu/TiO_2-L and Cu/TiO_2-H.

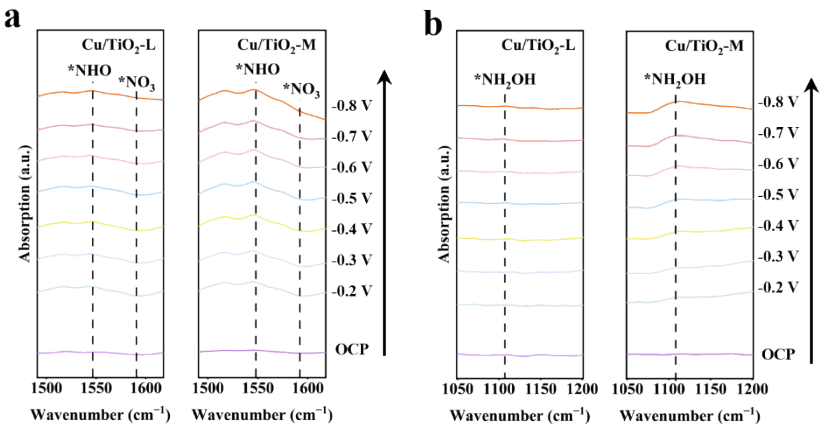

Figure S21. (a-b) The enlarged potential-resolved in-situ FT-IR spectra of (a) Cu/TiO_2-M and (b) Cu/TiO_2-L photoelectrodes.

Table S1. Comparison of Cu mass loading of Cu/TiO_2 photoelectrode.

Sample	Q (C)	m (mg)
Cu/TiO_2-L	−0.34	0.11
Cu/TiO_2-M	−1.08	0.36
Cu/TiO_2-H	−2.15	0.71

Notes: M=63.5 g mol^{-1}, n=2, F=96485 C mol^{-1}

Table S2. Potential-dependent NH_3 FE and production rate of Cu/TiO_2-M photoelectrode

E-iR_u	NH_3 Yield (mg h^{-1} cm^{-2})						FE (100%)					
	dark	positive deviations	negative deviations	light	positive deviations	negative deviations	dark	positive deviations	negative deviations	light	positive deviations	negative deviations
−0.3 V	0.107	0.001	−0.001	0.114	0.001	−0.001	37.5	0.5	−0.4	51.9	0.2	−0.2
−0.4 V	0.134	0.001	−0.001	0.213	0.002	−0.002	47.1	0.4	−0.5	65.2	0.6	−0.8
−0.5 V	0.230	0.003	−0.004	0.371	0.001	−0.001	63.6	0.8	−1.1	85.2	0.3	−0.2
−0.6 V	0.332	0.001	−0.001	0.477	0.005	−0.004	69.2	0.3	−0.2	82.1	0.8	−0.7
−0.7 V	0.343	0.004	−0.006	0.545	0.008	−0.006	58.0	0.6	−1.0	66.4	1.0	−0.8

Notes: The data points represent the median values, while the error bars indicate the positive and negative deviations.

Table S3. Comparison of NH_3 production rate and FE of Cu/TiO_2 photoelectrode

Sample	NH_3 Yield (mg h^{-1} cm^{-2})			FE (100%)		
	dark	positive deviations	negative deviations	light	positive deviations	negative deviations
TiO_2	0.065	0.001	−0.001	54.3	0.3	−0.6
Cu/TiO_2-L	0.133	0.003	−0.002	53.5	1.0	−0.6
Cu/TiO_2-M	0.371	0.001	−0.001	85.2	0.3	−0.2
Cu/TiO_2-H	0.274	0.003	−0.002	67.3	0.7	−0.5

Notes: The data points represent the median values, while the error bars indicate the positive and negative deviations.

Table S4. Comparisons on NO_3RR performances.

Photoelectro-Catalysts	Electrolyte	FE (%)	NH_3 yield rate	Ref.
Cu/TiO_2-M photoelectrode	0.1 M KOH 0.1 M KNO_3	85.2	0.38mg h^{-1} cm^{-2}	This Work
Other Catalysts				
$BiVO_4$/CuPc	0.5 M Na_2SO_4 100 ppm NO_3^--N	20.36	12.98 μg h^{-1} cm^{-2}	[1]
CuPc/CeO_2	0.1 M phosphate Buffer KNO_3	33	1.16 μmol h^{-1} cm^{-2}	[2]
Ni–Fe LDH/graphene/Si	0.5 M Na_2SO_4 100 mM $NaNO_3$	92.5	12.98 μg h^{-1} cm^{-2}	[3]
CoCu/TiO_2/Sb_2Se_3	10 mM H_2SO_4 100 mM KNO_3	88.01	15.91 μmol h^{-1} cm^{-2}	[4]
$ZnIn_2S_4$/$BiVO_4$	0.5 M Na_2SO_4 150 ppm NO_3^-	37.2	29.95 μg h^{-1} cm^{-2}	[5]
TiO_x/CdS/CZTS	10 mM H_2SO_4 100 mM KNO_3	89.1	8.21 μmol h^{-1} cm^{-2}	[6]
O_SiNW/Au	0.5 M K_2SO_4 100 mM KNO_3	95.6	0.26 μmol h^{-1} cm^{-2}	[7]
CeO_2-C/BiVO4	0.5 M Na_2SO_4 100 ppm NO_3^-	32.2	21.81 μg h^{-1} cm^{-2}	[8]
NiO/Au plasmon/TiO_2	0.2 M KNO_3	44	3 μmol h^{-1} cm^{-2}	[9]

Table S5. FE distribution of products over the Cu/TiO_2-M photoelectrode at various applied potentials.

E-iR_u	NH_3 FE (%)	NO_2^- FE (%)	H_2 FE (%)
−0.3 V	51.8	45.5	2.3
−0.4 V	65.1	33.0	1.7
−0.5 V	85.1	14.1	0.7
−0.6 V	82.0	16.5	1.3
−0.7 V	66.2	28.1	5.4

References

[1] Y.J. Bai, S.Y. Gao, W.R. Xie, Z.Y. Fang, H.Y. Bai, W.Q. Fan, Photoelectrochemical nitrate reduction to ammonia over $BiVO_4$/2D macromolecular with extremely low energy consumption, Int. J. Hydrog. Energy. 48 (2023) 10882-10890. http://dx.doi.org/10.1016/j.ijhydene.2022.11.329.

[2] X. Li, W.Q. Fan, Y.J. Bai, Y. Liu, F.F. Wang, H.Y. Bai, W.D. Shi, Photoelectrochemical reduction of nitrate to ammonia over CuPc/CeO_2 heterostructure: Understanding the synergistic effect between oxygen vacancies and Ce sites, Chem. Eng. J. 433 (2022) 8. http://dx.doi.org/10.1016/j.cej.2021.133225.

[3] C.H. Chiang, Y.T. Kao, P.H. Wu, T.R. Liu, J.W. Lin, P.T. Chen, J.W. Lin, S.C. Yang, H.L. Chen, S.B. Patil, D.Y. Wang, C.W. Chen, Efficient ammonia photosynthesis from nitrate by graphene/Si Schottky junction integrated with Ni-Fe LDH catalyst, J. Mater. Chem. A. 11 (2023) 11179-11186. http://dx.doi.org/10.1039/d3ta01169k.

[4] S.J. Ren, R.T. Gao, N.T. Nguyen, L. Wang, Enhanced Charge Carrier Dynamics on Sb_2Se_3 Photocathodes for Efficient Photoelectrochemical Nitrate Reduction to Ammonia, Angew. Chem.-Int. Edit. 63 (2024) 9. http://dx.doi.org/10.1002/anie.202317414.

[5] F.F. Wang, Q.J. Ding, J.R. Ding, Y.J. Bai, H.Y. Bai, W.Q. Fan, Frustrated Lewis pairs boosting photoelectrochemical nitrate reduction over $ZnIn_2S_4$/$BiVO_4$

heterostructure, Chem. Eng. J. 450 (2022) 10. http://dx.doi.org/10.1016/j.cej.2022.138260.

[6] S.J. Zhou, K.W. Sun, C.Y. Toe, J. Yin, J.L. Huang, Y.Y. Zeng, D.D. Zhang, W.J. Chen, O.F. Mohammed, X.J. Hao, R. Amal, Engineering a Kesterite-Based Photocathode for Photoelectrochemical Ammonia Synthesis from NO_x Reduction, Adv. Mater. 34 (2022) 11. http://dx.doi.org/10.1002/adma.202201670.

[7] H.E. Kim, J. Kim, E.C. Ra, H.M. Zhang, Y.J. Jang, J.S. Lee, Photoelectrochemical Nitrate Reduction to Ammonia on Ordered Silicon Nanowire Array Photocathodes, Angew. Chem.-Int. Edit. 61 (2022) 7. http://dx.doi.org/10.1002/anie.202204117.

[8] H.Y. Bai, F.F. Wang, Q.J. Ding, W.R. Xie, H.P. Li, G.L. Zheng, W.Q. Fan, Construction of Frustrated Lewis Pair Sites in CeO_2-C/$BiVO_4$ for Photoelectrochemical Nitrate Reduction, Inorg. Chem. 62 (2023) 2394-2403. http://dx.doi.org/10.1021/acs.inorgchem.2c04208.

[9] V.R. Silveira, R. Bericat-Vadell, J. Sá, Photoelectrocatalytic Conversion of Nitrates to Ammonia with Plasmon Hot Electrons, J. Phys. Chem. C. 127 (2023) 5425-5431. http://dx.doi.org/10.1021/acs.jpcc.3c00772.